

## Research Article

# Multifrequency Phase Difference of Arrival Range Measurement: Principle, Implementation, and Evaluation

Lanxin Qiu,<sup>1,2</sup> Zhangqin Huang,<sup>1,2</sup> Shaohua Zhang,<sup>1,2</sup> Cheng Jing,<sup>3</sup> Hao Li,<sup>4</sup> and Shuyao Li<sup>4</sup>

<sup>1</sup>Department of Software, Beijing University of Technology, Beijing 100124, China

<sup>2</sup>Beijing Engineering Technology Research Center for IoT Software and Systems, Beijing 100124, China

<sup>3</sup>Institute of Remote Sensing and Digital Earth, Chinese Academy of Sciences, Beijing 100094, China

<sup>4</sup>School of Electronic Engineering, Xidian University, Xi'an, Shaanxi 710071, China

Correspondence should be addressed to Zhangqin Huang; zhuang@bjut.edu.cn

Received 10 February 2015; Accepted 24 May 2015

Academic Editor: Dakshnamoorthy Manivannan

Copyright © 2015 Lanxin Qiu et al. This is an open access article distributed under the Creative Commons Attribution License, which permits unrestricted use, distribution, and reproduction in any medium, provided the original work is properly cited.

Real-time location system (RLS) based on RFID is an effective indoor positioning system. The battery-free and low cost UHF passive tags can be attached on almost any objects, which are recognized as the best medium to achieve high precision ranging and positioning for large-scale objects. This paper proposes an indoor range measurement based on multifrequency phase difference of arrival (MF-PDoA) using UHF RFID passive tags and discusses the measurement principle, experiment implementation, and results evaluation in detail. After a theoretical overview of MF-PDoA range measurement principle, it introduces an experimental prototype under EPC C1G2 standard for range measurements. Both our prototype and a commercial off-the-shelf RFID reader have been used to verify the measurement method. We propose a Kalman filter and weighting method to process the measuring data. Experiment results indicate that, in a real environment, this method can effectively improve the ranging accuracy, which lays a foundation to extend the proposed measurement into two to three dimensions indoor object positioning.

## 1. Introduction

Due to the rapid development of IoT technology, both intelligent devices and smart objects have rushed into our life and greatly affected our lifestyle. In 2020, each individual will be surrounded by over 1000 facilities, which are including not only our smart phones and different kinds of embedded system devices but also numerous articles of daily use with perceptible capability. The progress of large-scale intellectualized devices brings effective digital management challenge along with the convenience. Precise range and location information is the foundation to solve such problem, which is also the key to achieve intelligent control. Many applications would benefit from it such as products detection in large warehouse [1].

Since satellite-based ranging and positioning systems have been widely applied in outdoor environment, plenty of solutions have been proposed for indoor environment. Measurement system using WLAN and inertial sensor mixture signal makes advantage of multiple WLAN access points

as anchor nodes to navigate the mobile device, in which the inertial sensors such as accelerometer, gyroscope and magnetometer play a role as auxiliary calculation device to improve the ranging and positioning accuracy [2]. With the development of visible light communication technology (such as Light-Fidelity), mobile devices may have the ability to be navigated with visible light by integrating an optical sensor [3]. Although these solutions can make up the drawback of satellite-based positioning, they are still not applicable to give the range and location information for articles of daily use.

Radio Frequency Identification (RFID) system is considered to be a nonsubstitutable network access tool of the Internet of Things technology. It is generally composed of reader, reader antenna, and tags. According to the method of powering, the tags can be divided into active tag, passive tag, and semipassive tag [4]. Battery-free and low cost passive tags can be attached on almost any items, which are recognized as the best medium to achieve precise ranging and positioning for large-scale objects.

TABLE 1: Performance of the methods.

Method	Technology	Target	Accuracy	Infrastructure
Range-free measurement				
LANDMARK	$k$ nearest neighboring + weighting	Active	1 m+	Room
VIRM [7]	$k$ nearest neighboring + weighting	Active	21 cm–29 cm	Room
Kalman filter	RSS mean squares and Kalman filtering	Passive	60 cm–1 m	5 m * 5 m
Alippi et al. [8]	RSS Bayesian approach	Passive	68 cm	4 m * 5 m
Range measurement				
SpotON	RSS lateration	Active	Depend on cluster size	Cluster at least 3 tags
SAW ID-tags	TOA lateration	2.5 GHz passive	20 cm	7 m * 7 m
RSP	RSS/AOA	Passive	1.05°	1 m * 1 m
MD-PDoA (our prototype)	FD-PDoA + Kalman filter + weighting	Passive	13.5 cm	5 m * 5 m
MD-PDoA (COTS)	FD-PDoA + Kalman filter + weighting	Passive	15 cm	5 m * 5 m

In this paper, we present an indoor ranging measurement for passive RFID system based on multifrequency carrier phase difference of arrival (MF-PDoA). This approach is inspired by the multifrequency radar ranging system that the transmitter detects the distance from a receiver by measuring the phase differences generated from several transmission frequencies [5]. We try as completely as possible to explain the MF-PDoA method including the measurement principle, experiment implementation, and results evaluation. Both Kalman filter and weight data fusion method are applied for data progression. We also develop an experimental prototype under EPC C1G2 standard [6] and use both of our prototype and a commercial off-the-shelf RFID reader to verify the MF-PDoA method. It indicates that, in a real environment, this method can effectively improve the ranging accuracy, which lays a foundation to extend the proposed measurement into two to three dimensions indoor object positioning.

The organization of this paper is as follows. Section 2 shows some related works. The MF-PDoA ranging measurement principle is laid in Section 3. Establishment and implementation of the experimental prototype are in Section 4. Data procession is in Section 5 and results analysis is in Section 6. Section 7 is conclusion.

## 2. Related Works

The emergence of RFID indoor ranging and positioning technology is in 2000 and can be separated into two categories, which are range measurement methods and range-free measurement methods (see Table 1). Algorithm based on range measurement calculates the distance or angle between the reader and tag to know the target position; a classic system is SpotON [9]. LANDMARC [10] is a popular range-free positioning system, which compares the similarity and relevancy of the target tag to the anchor nodes to indirectly give the target position. In this way, the range-free algorithms need a number of reference tags with known positions. Both of high environment complexity and implementation costs make such methods are not conducive in the practical application.

Excepting our phase-based measurement system, the range measurement approach can be divided into signal time

of arrival (ToA), signal time difference of arrival (TDoA), signal angle of arrival (AoA), and received signal strength indicator (RSSI) according to the measuring characteristic information [4]. Indoor environment is a complex multipath Non-Line-of-Sight (NLOS) environment. When using TOA or TDOA methods, the RFID system needs to generate nanosecond level time to ensure the location measurement accuracy, but it is difficult to achieve. In addition, the AoA-based method needs additional hardware like phased array antennas in an open space.

RSSI based methods use Path Loss Model [11] to establish the range measurement model. However, ranging method based on the Path Loss Model cannot be applied mechanically under real environment. Due to the indoor impact on RF reflection and multipath effect, RSSI fluctuation interval generally exists and the measurement is hard to remain at a high accuracy level. To prove this situation, we carry out an experiment by using ImpinJ Speedway R420 UHF commercial off-the-shelf reader, Laird S9028 9 dBi cycle polarization antenna [12], and ImpinJ Monza tag [13]. The tag was planned to move 18 steps from 0.5 m to 4 m, at a step size of 0.2 m, away from the reader antenna. At each position, we collect 200 RSSI samples and demonstrate the RSSI value distribution in Figure 1. It clearly indicates the RSSI fluctuation interval is about 12 dBm. In addition, Figure 2 is the RSSI normalization distribution of two different positions. The distributions are independent of each other. They can either obey Gaussian distribution or not, which all depend on the environment complexity. The randomness of multipath reflection and interference make it even harder to generalize or summarize the relationship between the RSS distribution rule to the tag-to-reader distance. Thus, we aim to use phase based method to give more accurate and precise ranging result.

## 3. Range Measurement Principle

**3.1. RFID Signal Delay Model.** The RFID reader transmission carrier wave signal is a continuous wave (CW) signal. The ranging measurement based on phase difference of arrival is to use the phase change of the propagation path between the reader to the tag, corresponding to determine the tag-reader distance.

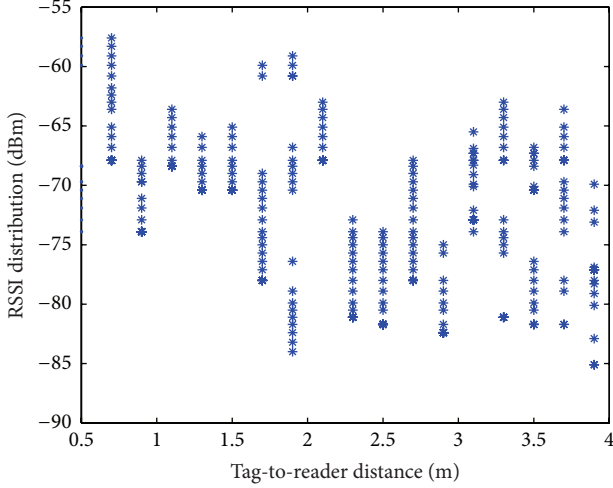


FIGURE 1: RSSI distribution versus distance (ImpinJ Monza).

Figure 3 shows the passive RFID system signal transmission model. In the ideal situation, the reader transmitting signal phase  $\theta_t$  at time  $t$  can be regarded as the initial phase and assigned to zero. After a period of time, the tag reflects the signal back to the reader at time  $k$  with the receiving signal phase  $\theta_k$ . The phase difference can be described as

$$\theta = \theta_k - \theta_t = \theta_k. \quad (1)$$

Here  $\theta$  is the whole signal phase delay during the integrated communication process. Excepting the propagation phase delay ( $\theta_d$ ), the reader's transmitter circuits ( $\theta_{tc}$ ), the receiver circuits ( $\theta_{rc}$ ), and the tag's reflection characteristic ( $\theta_{tag}$ ) will all introduce additional phase rotation. We have

$$\theta = \theta_d + \theta_{tc} + \theta_{rc} + \theta_{tag}, \quad (2)$$

where the propagation phase delay can be calculated by

$$\theta_d = 2\pi \cdot \left( \frac{2d \cdot f}{c} \right). \quad (3)$$

$d$  is the distance from the transmitter to receiver at carrier wave frequency  $f$ , and the total distance of the backscattered signal travelling between the reader and the tag is  $2d$ .

**3.2. The Phase Difference Ranging Measurement Principle.** As the formula discussed above, the distance between the reader and tag can be calculated as

$$d = \frac{c \cdot \theta_d}{4\pi \cdot f}. \quad (4)$$

However, the reader can only detect the receiving signal phase value  $\theta_k$  (equal to phase delay  $\theta$ ) instead of  $\theta_d$ , which leads to a measurement deviation. What is more, the phase delay  $\theta$  is a periodic function with  $2\pi$  radians while the measured phase value by the reader is  $\theta \bmod (2\pi)$ . If the tag-to-reader distance is larger than  $R_{\max} = c/2f$ , which is referred as the maximum unambiguous range, the phase

difference exceeds  $2\pi$  and brings phase warping. It is a critical issue in range estimation when the maximum possible range is relatively large [14]. For example, when the transmission frequency is 900 MHz, the unambiguous range is 16.2 cm which means the phase warping is a ubiquitous existing problem.

We achieve this by using the concept of phase difference of arrival (PDoA). There are three main techniques based on phase difference of arrival, which are Time Domain PDoA (TD-PDoA), Frequency Domain PDoA (FD-PDoA), and Spatial Domain PDoA (SD-PDoA) in [15]. We adopt the second technology by measuring the phase of the tag signal at multifrequency. The range to tag can be calculated as

$$d = \frac{c}{4\pi} \cdot \frac{\Delta\theta}{\Delta f}, \quad (5)$$

where  $\Delta\theta$  denotes the detected phase variation when two-carrier wave frequency variation is  $\Delta f$ . Interference elements  $\theta_d$ ,  $\theta_{tc}$ , and  $\theta_{rc}$  are nearly constant and can be removed out from the result by multiple phase difference measurement. Additionally, adequate frequency separation can be chosen to accommodate the unambiguity range estimation. If we select  $\Delta f = 1$  MHz to solve the phase value calibration problem, the phase ambiguity appears at the distance  $d = c/2f = 150$  m, which is much larger than the passive RFID communication range (smaller than 15 m).

However, when in the real environment, the transmitting signal phase is always nonzero. It is dependent on the measurement system hardware characteristics. We define a calibration distance denoted  $d_{\text{cor}}$  to describe the influence and change the final formula as below.  $d_{\text{cor}}$  calculation will be discussed later:

$$d = \frac{c}{4\pi} \cdot \frac{\Delta\theta}{\Delta f} - d_{\text{cor}}. \quad (6)$$

**3.3. Extend to 2D Space Positioning.** It is possible to extend the MF-PDoA method to 2D or 3D space positioning by using multiple receivers. A multiple input multiple output (MIMO) system consisted of one reader and two antennas for both transmitting and receiving shown in Figure 4. We denote the antenna to reader distance as  $r$  the range estimation  $d_1$  and  $d_2$  from MF-PDoA method are equivalent to the radii of each ellipse. The intersections of these two ellipses can be found by solving a geometrical problem and the target tag distance is

$$d = \sqrt{\frac{d_1^2 + d_2^2 - 2r^2}{2}}. \quad (7)$$

## 4. Prototype Implementation

Range measurement as the foundation of positioning will be discussed later. In this chapter, we firstly describe and simulate the quadrature signal demodulation phase measurement method. Then, we establish our prototype by using an ImpinJ R2000 UHF RFID SoC chip and a FPGA chip which integrates an analogy to digital converter. Physical level quadrature demodulation waves of the tag reflection signal

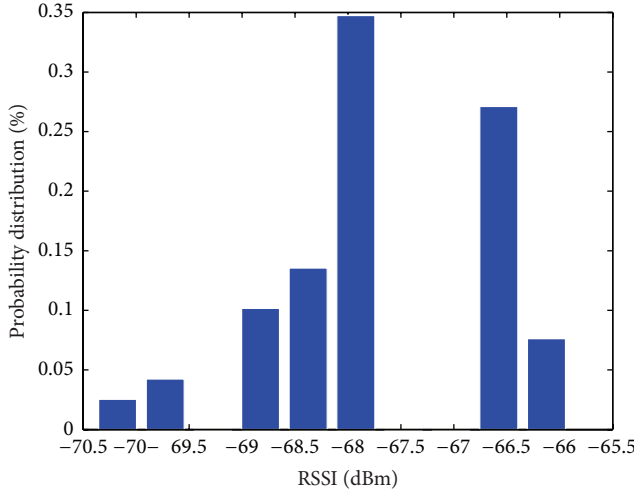


FIGURE 2: RSSI distribution versus position (ImpinJ Monza).

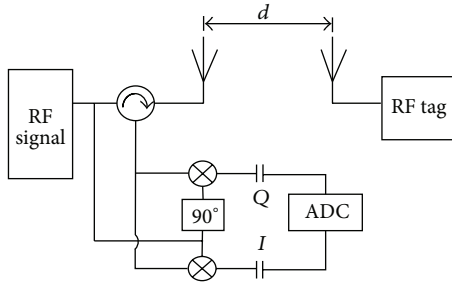
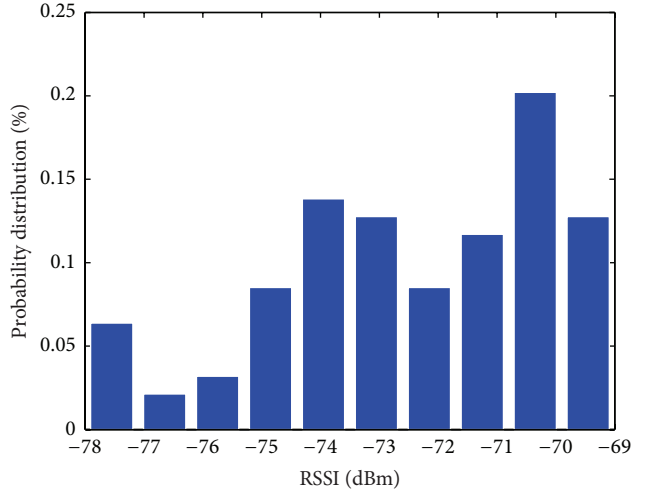


FIGURE 3: RFID system signal transmission model.

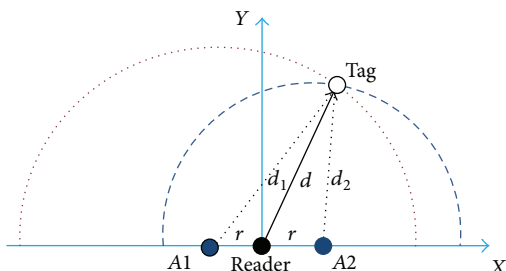


FIGURE 4: 2D positioning model.

are received by the R2000 RFID front-end chip and the FPGA chip samples the signal strength amplitude to calculate the phase of arrival.

**4.1. Phase Simulation.** In a typical wireless communication system, the phase measurements include FFT phase detecting method, coherent demodulation method, and so forth. The passive RFID system belongs to zero intermediate frequency system, which means the receiving signal carrier wave frequency is consistent with the local oscillator frequency. By respectively demodulating the quadrature signals with local oscillator signal, we can acquire the phase value and avoid the phase blind spots at the same time. Figure 5 is our simulation

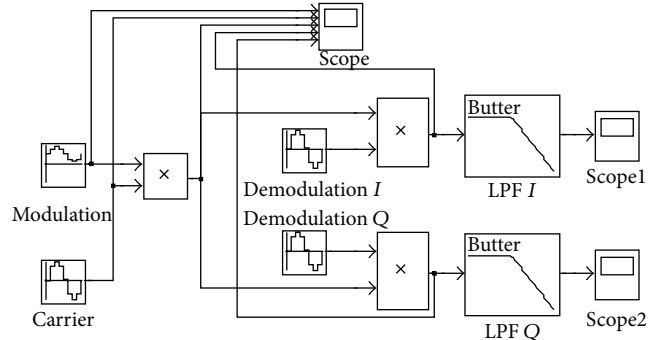


FIGURE 5: Quadrature demodulation system.

system in MATLAB which indicates the quadrature demodulation scheme. Two orthogonal vibration signals, respectively, are demodulated with the receiving signal. The demodulated I/Q wave is the system output results.

Denoting the carrier signal as  $\cos(\omega t)$  (with frequency  $f$ ), the system receiving signal is  $A \cos(\omega_0 t) \cos(\omega t + \theta)$ , where  $f_0$  is the modulation signal frequency ( $\omega_0 = 2\pi f_0$ ). According to the communication standard, we have  $f \gg f_0$ . Phase difference between the receiving signal and the transmitting signal, for example,  $\theta$ , can be calculated according to the triangle formula and demodulation principle; here,

$$\begin{aligned}
 I' &= \left( \frac{A}{2} \right) \cdot \cos \omega_0 t \cdot \cos (2\omega t + \theta) + \left( \frac{A}{2} \right) \cdot \cos \omega_0 t \\
 &\quad \cdot \cos \theta, \\
 Q' &= \left( \frac{A}{2} \right) \cdot \cos \omega_0 t \cdot \sin (2\omega t + \theta) - \left( \frac{A}{2} \right) \cdot \cos \omega_0 t \\
 &\quad \cdot \sin \theta.
 \end{aligned} \tag{8}$$

After filtering out the high frequency components by the low pass filter, the signal can be described as

$$\begin{aligned} I &= \left( \frac{A}{2} \right) \cdot \cos \theta \cdot \cos \omega_0 t, \\ Q &= -\left( \frac{A}{2} \right) \cdot \sin \theta \cos \omega_0 t. \end{aligned} \quad (9)$$

Then, the phase  $\theta$  can be calculated as

$$\theta = \arctan \left( -\frac{Q}{I} \right), \quad \theta \in \left( -\frac{\pi}{2}, \frac{\pi}{2} \right). \quad (10)$$

The real modulation frequency and carrier frequency of UHF RFID system are not appropriate for simulating observation. We use lower frequency for the  $IQ$  demodulation process under ideal environment to illustrate the theory. The modulation frequency is 6 Hz with 1 V amplitude and 3 V bias. The initial phase of modulation wave does not affect the demodulation results and we give it to zero. The carrier wave is 90 Hz with 5 V amplitude and no bias. The two orthogonal vibration demodulation waves are as the same frequency as carrier wave, but with 1 V amplitude and quadrature phase value ( $0^\circ$  for  $I$  and  $90^\circ$  for  $Q$ ).

In our system, all the waves are cosine wave and the phase unit is  $\text{rad}(2\pi = 360^\circ)$ . The two Butterworth Low Pass Filters are exactly the same with 8 Hz pass band frequency (they should be in the range from  $f_0$  to  $2f_0$ ). We can see that the wave forms with initial phase ( $60^\circ$  and  $240^\circ$ ) are almost the same but with opposite amplitude. From (9), we know  $\cos(\omega_0 t)$  is a constant. So after filtering the high frequency composition, there is only amplitude difference without phase difference of the  $IQ$  signals in Figures 6(b) and 6(c).

By using the Scope data recording function in Simulink, we import the  $I/Q$  sampling data into Matlab and calculate the carrier phase value by (10). The initial carrier wave phase is, respectively, configured as  $0^\circ$ ,  $60^\circ$ ,  $120^\circ$ , and  $240^\circ$ , which can be explained as a result of the transmission distance delay. As shown in Figure 7, the calculated phase values are correct and belong to  $(-\pi/2, \pi/2)$ . When the carrier wave phase is  $60^\circ$  and  $240^\circ$ , the calculated values are the same. This obviously reveals a drawback of arctangent phase acquiring method, the phase ambiguity [16]. We will talk about the influence of this phenomenon in the subsequent chapters.

**4.2. Prototype Implementation.** ImpinJ Indy R2000 UHF RFID reader chip is a highly integrated, high-performance device for EPC Class1 Gen2 applications. It supports zero intermediate frequency (ZIF) architecture of the worldwide ISM band (the operating frequencies are from 840 MHz to 960 MHz). The Indy R2000 reader chip comprises all of the RF and Baseband blocks to interrogate and receive data from compatible RFID tags. The transmitter supports both in-phase quadrature ( $IQ$ ) vector modulation and polar modulation. Figure 8 is the overall block diagram of the R2000 chip [13].

Indy R2000 chip provides analog test function to observe and analyze quadrature signal. By configuring the internal

register (register address x0430 according to the ImpinJ technology support), we can flexibly choose the analog test pin to show the signal wave from LNA or low pass filter directly from the RF front end. The experiment is established in Figure 9(a); despite an oscilloscope, we can see the physical level  $IQ$  signal. The yellow line in Figure 9(c) shows  $I$  channel and the blue one is the  $Q$  channel. The signal wave clearly shows the modulation frequency is 250 kHz and the T-R modulation scheme is miller-4. As analysis in the early chapter shows, the quadrature channel only has the amplitude difference. A Xilinx Zynq [17] chip with 12-bit ADC block can be used to capture the tag receiving  $I/Q$  quadrature analog signals and convert them into digital form to detect the amplify change with variable carrier frequencies and tag distance. The hardware system structure development of Zynq in Vivado SDK shows in Figure 10. Differential analog input of  $I/Q$  signals from R2000 text pins are sent to ADC block for sampling. 12-bit ADC separates the amplitude into 4096 shares, which also means the phase calculating precision is at least  $0.08^\circ$ . Amplitude results of  $I/Q$  channel are sent through the serial port to PC for display in Figure 11. According to (10), phase of arrival can be calculated by the amplitude radio.

We give the amplitude statistic data in Figure 12 when the tag-to-reader distance is constant along with frequency increasing. We can see that when the frequency is increasing, the receiving signal package is harder to be detected, which decreases the phase sampling accuracy. It is because the output signal from quadrature demodulator is interfered by channel noise. It is desirable to recover RSS sign using the phase information contained in the Baseband signal and a Goertzel's algorithm method to acquire more accurate phase value is put forward in [18, 19]. However, in this paper, we simply choose 900–920 MHz which has a relatively stable RSS value to estimate the distance.

**4.3. Phase Measurement Using Our Prototype.** Measurements have been performed by a Larid 9028 9 dBi antenna and ImpinJ Monza tag (see Figure 16). The tag was planned to move 30 steps from 0.5 m to 3.5 m, at a step size of 10 mm, away from the reader antenna. At each position, our prototype uses multiple transmission carrier wave frequencies to collect phase information. At least 200 tag phase values are recorded corresponding to each frequency. Experiment results in Figure 13(a) show the phase distribution when the distance is 2.2 m and the carrier wave frequency is 907 MHz, which indicates the phase values for a same carrier wave frequency obey to Gaussian distribution (normalization processed). Figure 13(b) shows the phase distribution when carrier wave frequency changes from 913 MHz to 920 MHz at 2.2 m. We can see the phase value linearly changes with the carrier wave frequency.

Considering the drawback of the arctangent phase acquiring method, the phase ambiguity also exists in our system. When operating the inventory command, we give a phase value pair including a small phase value and a large phase value with  $\pi$  difference at the same time. Although there is no method to directly distinct these numbers as which one

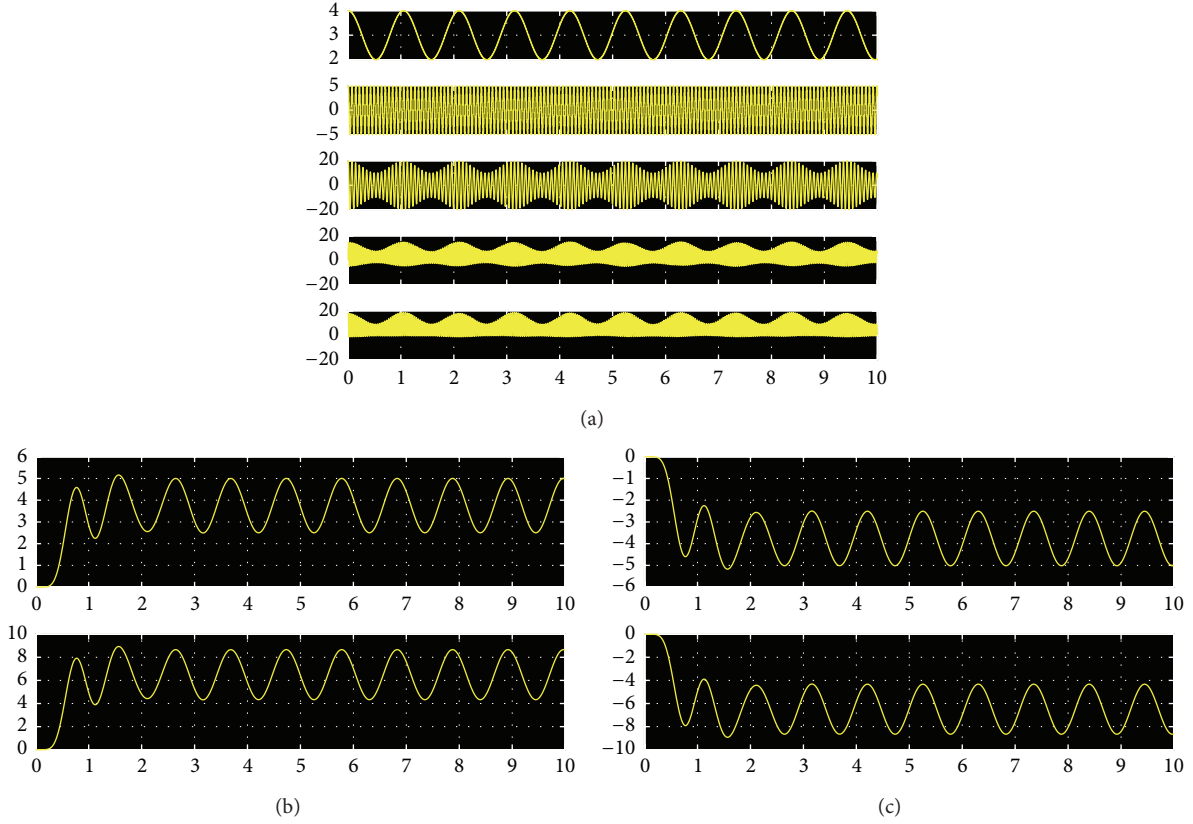


FIGURE 6: (a) Quadrature demodulation system results in Scope window: the wave form of the modulation wave, carrier wave, AM wave, and the quadrature demodulation wave. (b) The wave form of the quadrature demodulation system results from LBF in Scope1 and Scope2 when the initial phase is  $60^\circ$ . (c) The wave form of the quadrature demodulation system results from LBF in Scope1 and Scope2 when the initial phase is  $240^\circ$ .

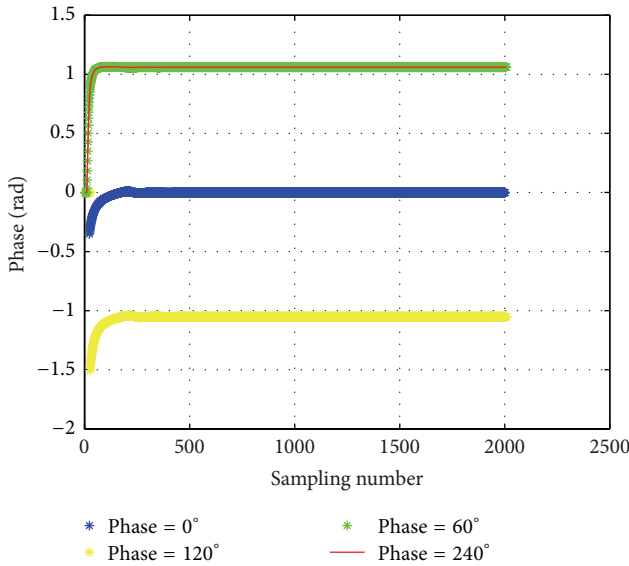


FIGURE 7: Phase values simulation.

is correct, we comprehensively analyze them in context with other frequency phase values. For example, if the phase pairs

are  $170^\circ$  and  $350^\circ$  at 915 MHz,  $182^\circ$  and  $2^\circ$  at 916 MHz, and  $194^\circ$  and  $14^\circ$  at 917 MHz, we can use  $170^\circ$ ,  $182^\circ$ , and  $194^\circ$  to calculate the phase difference or pick  $350^\circ$ ,  $2^\circ$ , and  $14^\circ$  with the same effect. On the other hand, the advantage of R2000 chip is the long selectable carrier frequency range, from 840 MHz to 960 MHz, which supplies us with an opportunity to collect phase value from more frequency channels.

## 5. Measurement Data Procession

Now, by establishing the phase measurement prototype, arrival phase value of the tag reflecting signal can be detected. Before developing the range measurement experiment, Kalman filter has been used to calibrate the phase difference value (see Figure 15). A weight data fusion method has also been proposed to improve the range estimation accuracy and system robustness.

**5.1. Kalman Filter Phase Difference Calibration.** We use multifrequency to obtain multiple phase difference value. The frequency separation can be either the same or not. According to the phase sampling deviation and the complex multipath interference, the phase difference values are floating as in Figure 13(b). To improve the ranging accuracy, we use

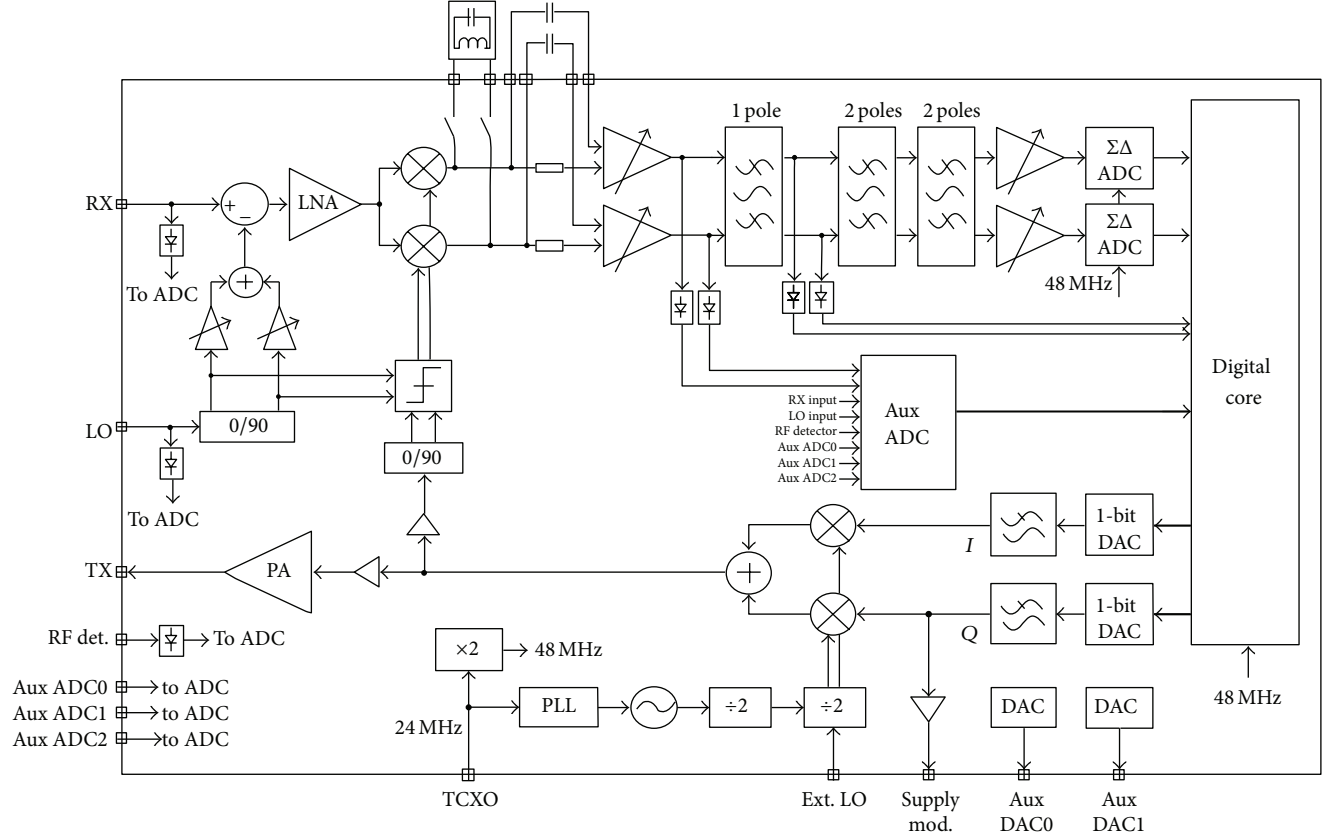
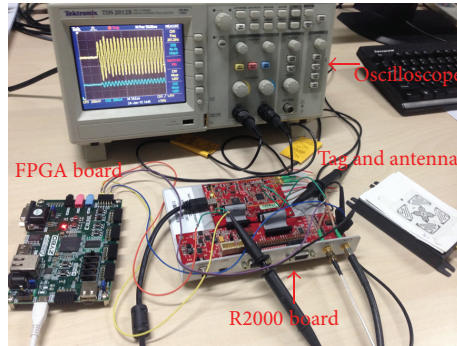


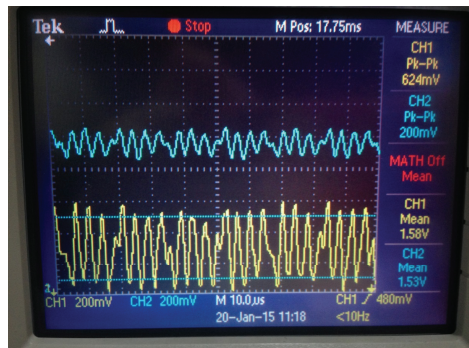
FIGURE 8: ImpinJ R2000 reader chip top level block diagram.



(a)

Number	Description	Parameter
1	R → T modulation	PR-ASK
2	T → R modulation	Miller-4
3	Tari length	Tari = 25 $\mu$ s
4	R → T calibration	RTcal = 62.5 $\mu$ s
5	T → R calibration	TRcal = 85.33 $\mu$ s
6	Use pilot tone	Trext = 1
7	Low frequency	LF = 250 kHz
8	Time slot number	Q = 0
9	Inventoried session	Session = S0
10	Inventoried flag	Target = A

(b)



(c)

FIGURE 9: (a) The ImpinJ R2000 development board experiment. (b) The protocol configuration parameters. (c) IQ signal wave in oscilloscope.

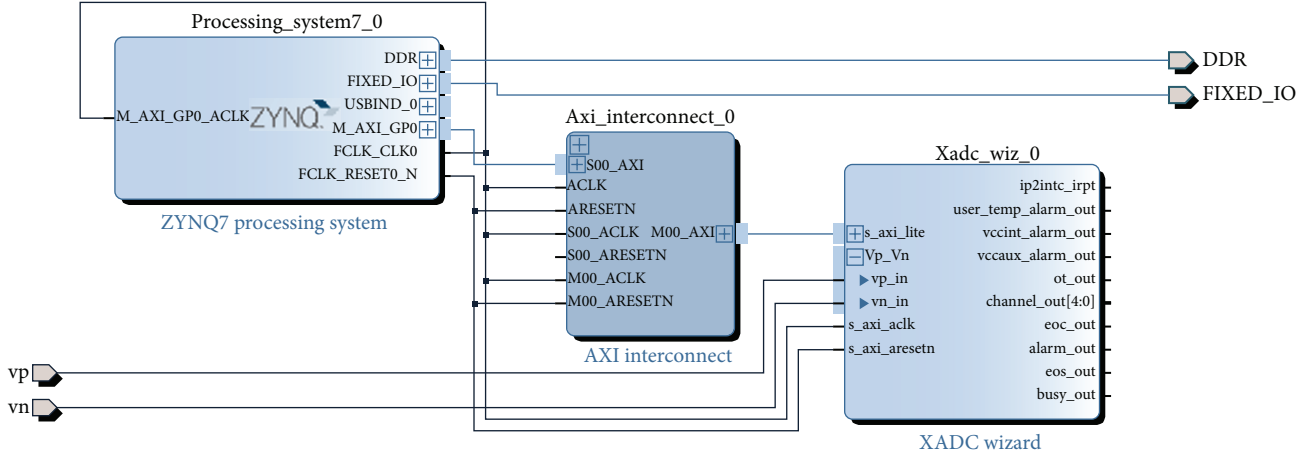


FIGURE 10: Zynq hardware structure.

```
//ADC initialization
ConfigPtr = XadcPs_LookupConfig(XPAR_AXI_XADC_0_DEVICE_ID);
if (ConfigPtr == NULL)
{
    return XST_FAILURE;
}
Status_ADC = XadcPs_CfgInitialize(XADCInstPtr, ConfigPtr, ConfigPtr->BaseAddress);
if(XST_SUCCESS != Status_ADC)
{
}
```

Serial: (COM7, 115200, 8, 1, None, None - CLOSED) - Encoding: (ISO-8859-1)

```
Raw VccI 3248 Real VccI 1.4372
Raw VccQ 2170 Real VccQ 0.9937
Raw VccI 3265 Real VccI 1.4348
Raw VccQ 2171 Real VccQ 0.9942
Raw VccI 3213 Real VccI 1.4119
Raw VccQ 2170 Real VccQ 0.9937
Raw VccI 3211 Real VccI 1.4109
Raw VccQ 2165 Real VccQ 0.9911
```

FIGURE 11: I/Q signal amplitude sampling results.

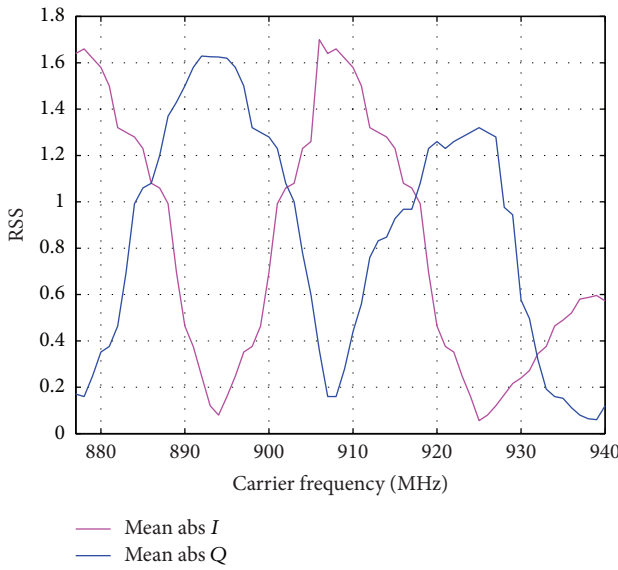


FIGURE 12: RSS value with frequency increasing.

Kalman filter to calibrate the phase difference value. Kalman filter [20] is wildly used in discrete data linear filtering problem. Our passive RFID PDoA range measurement system can be abstracted to a linear stochastic differential system

and use Kalman filter to obtain an optimum phase difference from the multiple phase values to improve the measuring accuracy. Denote the carrier frequency is  $f_1, f_2, \dots, f_n$ , 200 detected phase values under each carrier frequency follow  $N(\theta(i), \sigma(i))$  distribution. A total number of  $m = n * (n - 1)/2$  phase difference values can be produced by arbitrary two frequencies. Assuming  $\theta(k)$  ( $k$  from  $[1, m]$ ) is the  $k$ th real phase difference of  $f_i$  and  $f_j$ ,  $\theta(k - 1)$  is the  $(k - 1)$ th real phase difference,  $z(k)$  is the  $k$ th experiment phase difference with random error  $V(k)$ .  $V(k)$  is a white Gaussian noise, with covariance  $v(k)$ . We have

$$\begin{aligned} \theta(k) &= \theta(k - 1), \\ z(k) &= \theta(k) + V(k). \end{aligned} \quad (11)$$

According to Kalman Filter theory,  $\theta(k - 1 \mid k - 1)$  is the previous optimum estimation phase difference result; it equals the next predicted phase difference, either of its covariance

$$\begin{aligned} \theta(k \mid k - 1) &= \theta(k - 1 \mid k - 1), \\ p(k \mid k - 1) &= p(k - 1 \mid k - 1). \end{aligned} \quad (12)$$

Combining the  $k$ th experiment phase value  $z(k)$  with the predicted value, we can obtain the  $k$ th optimum phase difference value as below:

$$\begin{aligned} \theta(k \mid k) &= \theta(k \mid k - 1) \\ &\quad + kg(k)(z(k) - \theta(k \mid k - 1)), \\ kg(k) &= \frac{p(k \mid k - 1)}{(p(k \mid k - 1) + v(k))}, \\ p(k \mid k) &= (1 - kg(k))p(k \mid k - 1). \end{aligned} \quad (13)$$

By giving the initial values  $\theta(1 \mid 1)$  and  $p(1 \mid 1)$ , the Kalman filter can iterate to obtain the final optimum phase difference value.

Kalman filter (12) to (13) is used to estimate an optimum phase difference. The initial value  $p(1 \mid 1)$  is configured to

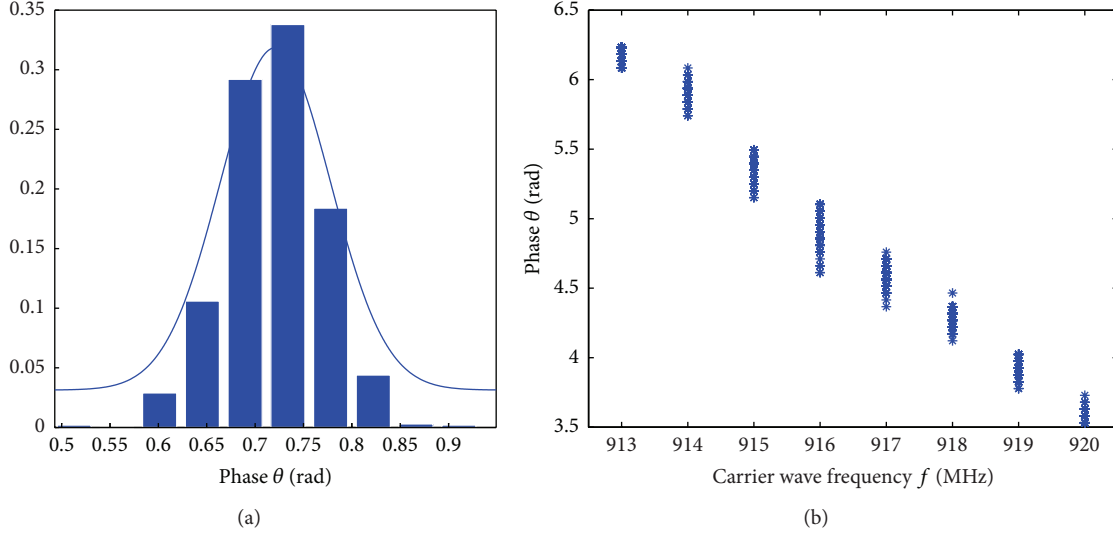


FIGURE 13: (a) Phase value distribution  $f = 907$  MHz at 2.2 m (ImpinJ Monza). (b) Phase value distribution  $f = 913$  MHz to 920 MHz at 2.2 m (ImpinJ Monza).

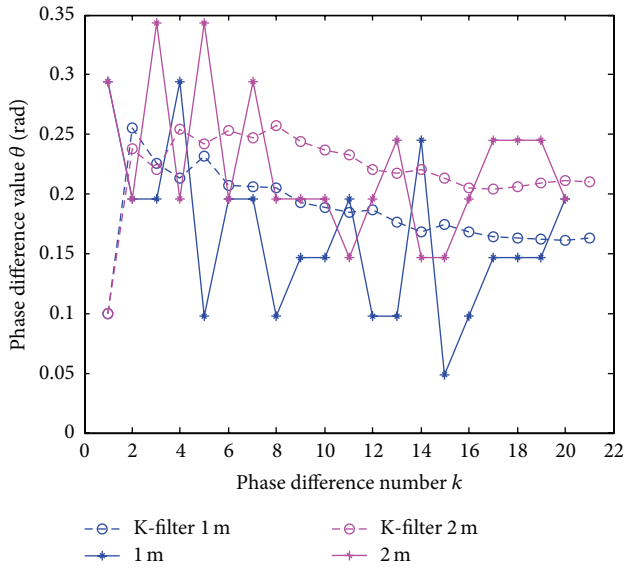


FIGURE 14: Influence of Kalman filter.

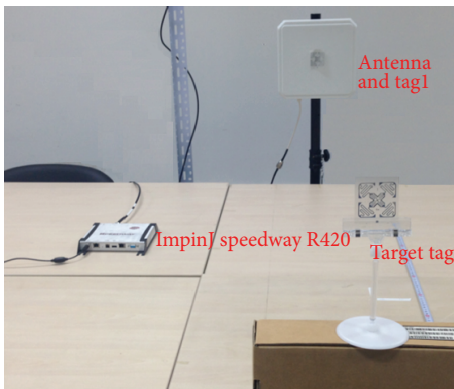


FIGURE 15: ImpinJ R420 reader range measurement experiment.

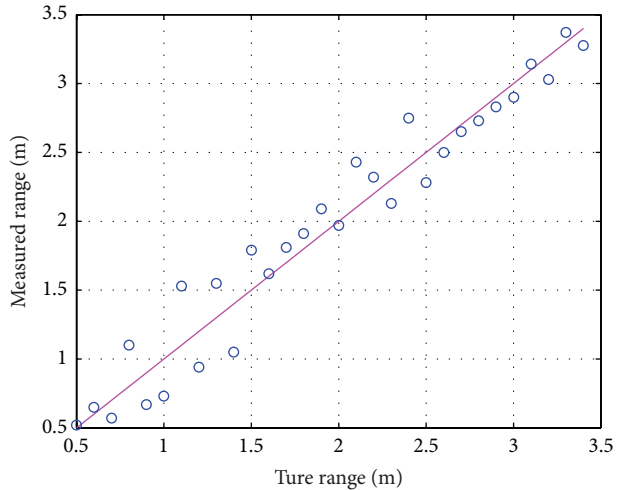


FIGURE 16: Ranging results of our prototype (ImpinJ Monza).

be 0.1. The difference between the maximum and minimum phases difference value is set to be the initial  $p(1 \mid 1)$ .  $v(k)$  is the sum of two carrier wave phase covariances  $\sigma(i)$  and  $\sigma(j)$ . For example, the maximum and minimum phases difference value of  $z(1)$  from  $z(20)$  is 0.5, which equals  $p(1 \mid 1)$ . The corresponding phase value covariance of 904 MHz and 905 MHz carrier waves is 0.03 and 0.04; then, the covariance  $v(1)$  is 0.05. Taking all these values of  $\theta(1 \mid 1)$ ,  $p(1 \mid 1)$ ,  $v(1)$  into (12) and (13) we can obtain the estimation phase difference values  $\theta(2 \mid 2)$  and  $p(2 \mid 2)$  and start the next iteration step. Figure 14 shows the phase difference value before and after Kalman filter when tag is at 1 m and 2 m. It shows that the phase difference value is more smooth and reliable after K-filter and the phase difference at 2 m is larger. We select the last phase difference value as the optimum one to estimate the distance by (6).

**5.2. Weight Data Fusion Distance Calibration.** If we separate the phase difference values into several clusters according to the frequency difference to calculate distance, a group of range estimation results can be fused to improve the robustness against noise and system propagation characteristics. Unlike the fixed frequency separation in [18], we propose to use different frequency separation to have varying level of range estimation quality. It is desirable to have weighted average of the range estimation rather than simple averaging. For our prototype, we choose the largest frequency pair variation as 4 MHz and ambiguity range issue will not happen in our experiment.

Estimation volume is the fusion distance  $\hat{d}$ . Several calculating distance values are independent of each other;  $w_{ij}$  is the weight data. Higher weight means a high influence to the real distance. We have

$$\hat{d} = \sum_{i=1}^n \sum_{j=i+1}^n w_{ij} \cdot d_{ij} \quad \text{where } \sum_{i=1}^n \sum_{j=i+1}^n w_{ij} = 1. \quad (14)$$

According to [21], the range estimates using the frequency pairs with larger separations are insensitive to noise and thereby have higher estimation accuracy. Therefore, the weight of the large separation pair could take a higher value in the fusion to improve the accuracy. In particular, we give the weight data as

$$w_{ij} = \frac{f_{ij}}{\sum_{u < v} f_{uv}}. \quad (15)$$

**5.3. Calibration Distance Estimation.** As mentioned above, when, in the real environment, the transmitting signal phase is always nonzero, it is incorporated in environment calibration distance  $d_{cor}$ , which is a correction distance. It can be obtained as an average of differences between real distances and measured distance. Another method is to adhere an auxiliary tag on the surface of the reader antenna center to calculate. We invent this auxiliary tag along with the target tag to collect phase value under each frequency. Then,  $d_{cor}$  can be set as the fusion distance from (14) by using auxiliary tag phase value. The ultimate range measurement result equals the difference between target tag fusion distance and calibration distance.

## 6. Experiment Implementation and Results

Measurements have been performed using a Larid 9028 9 dBi antenna and an ImpinJ Monza tag pair. Excepting our prototype, we also use a commercial off-the-shelf UHF RFID reader ImpinJ speedway R420 without any hardware or firmware modification to do the range measurement experiment. By adopting LLRP communication protocol [22] and enabling the extension parameters, the ImpinJ reader can support the phase report with the received information package [23]. We adjust the reader configuration to immediately report reading whenever tag is detected. The software is implemented using C#. It has a same phase sampling precision with our prototype. However, according to the

regulatory region control and the firmware configuration, we can only use Chinese region to operate 16 fixable frequency channels from 920.625 MHz to 924.375 MHz with 250 kHz step.

The communication protocol parameter configuration is mostly unchanged as described in Figure 9(b) without  $Q = 1$ . All the tag movement positions and reader antenna positions in experiments for the two hardware platforms are the same. At each position, 80 transmission channels from 900–920 MHz and 5 phase difference clusters corresponding to 250 kHz, 500 kHz, 1 MHz, 2 MHz, and 4 MHz frequency differences are considered to improve the range estimation result by using our prototype, while 16 channels and 3 clusters corresponding to 250 kHz, 500 kHz, and 1 MHz are considered for the COTS reader. 200 phase samples at each frequency are recorded. The phase ambiguity solution to COTS reader is identical with our prototype.

We use the root mean square deviation (RMSD) [24] to measure the accuracy of tag estimation range. Where  $N$  is the total estimation number,  $\hat{d}_N$  is the real distance, and  $d_N$  is the calculating distance:

$$\text{RMSD}(\hat{d}_N) = \sqrt{\frac{1}{N} \sum_{i=1}^N (|d_N - \hat{d}_N|^2)}. \quad (16)$$

To analyze the performance, we compare with the exiting ranging and positioning method like LANDMARK, SpotON, and SAW mentioned in [4]. Popularity, standardization, and performance are considered to choose the reference algorithms. The average calculation distance of our prototype is 3.385 m and 3.16 m for R420 system. The RMSD of the ranging estimation of our prototype from 0.5 m to 3.5 m is 13.5 cm with minimum error 1.3 cm, while the accuracy of R420 is 15 cm with minimum 6 cm. Better accuracy of our prototype is benefit from a larger number of phase sampling from more frequency channels. Ranging inaccuracy is caused by the phase sampling deviation, imperfect hardware,  $d_{cor}$  variation over temperature, radio wave reflection, reference in the environment, and so forth. The range measurements were repeated several times for different tag angle. The range measurement shows a tag angle insensitivity, which is also implied in [23].

## 7. Conclusion

In this paper, we have focused on the multifrequency phase difference of arrival range measurement method for passive UHF RFID system. We try as completely as possible to explain the experiment implementation and results evaluation. Both Kalman filter and weight data fusion method are applied for data progression. Experiment results indicate that MF-PDoA method has a certain uniformity and generality with better ranging accuracy. The future work is to use multiple transmission reader antennas and expands this range measurement to 2D and 3D space indoor localization. Multiple target tags and moving tag scenario will also be considered. Large-scale objects ranging and positioning involved applications like products detection in large warehouse would benefit from it.

## Conflict of Interests

The authors declare that there is no conflict of interests regarding the publication of this paper.

## Acknowledgment

This research is supported by Beijing Natural Science Foundation (no. 4122010) and Beijing Science and Technology Innovation Platform Program (nos. PXM2014\_014204\_07\_000049, PXM2015\_014204\_500211).

## References

- [1] J. Wang and D. Katabi, "Dude, where's my card?: RFID positioning that works with multipath and non-line of sight," *ACM SIGCOMM Computer Communication Review*, vol. 43, no. 4, pp. 51–62, 2013.
- [2] Z. Xiao, H. Wen, A. Markham, and N. Trigoni, "Lightweight map matching for indoor localisation using conditional random fields," in *Proceedings of the 13th ACM/IEEE International conference on Information Processing in Sensor Networks (IPSN '14)*, pp. 131–142, Berlin, Germany, April 2014.
- [3] P. Hu, L. Li, C. Peng, G. Shen, and F. Zhao, "Pharos: enable physical analytics through visible light based indoor localization," in *Proceedings of the International Conference of Hotnets*, November 2013.
- [4] M. Bouet and A. L. dos Santos, "RFID tags: positioning principles and localization techniques," in *Proceedings of the 1st IFIP Wireless Days (WD '08)*, November 2008.
- [5] J. L. Eaves and E. K. Reedy, *Principles of Modern Radar*, Van Nostrand Reinhold, New York, NY, USA, 1987.
- [6] EPCglobal, *EPC Radio-Frequency Identification Protocols Class-1 Generation-2 UHF RFID Protocol for Communications at 860 MHz–960 MHz, Ver. 2.2.0.0*, EPCglobal, 2013.
- [7] J. Han, Y. Zhao, Y. S. Cheng, T. L. Wong, and C. H. Wong, "Improving accuracy for 3D RFID localization," *International Journal of Distributed Sensor Networks*, vol. 2012, Article ID 865184, 9 pages, 2012.
- [8] C. Alippi, D. Cogliati, and G. Vanini, "A statistical approach to localize passive RFIDs," in *Proceedings of the IEEE International Symposium on Circuits and Systems (ISCAS'06)*, IEEE, Kos, Greece, May 2006.
- [9] J. Hightower, R. Want, and G. Borriello, "SpotON: an indoor 3D location sensing technology based on RF signal strength," Tech. Rep. UW CSE 00-02-02, Department of Computer Science and Engineering, University of Washington, 2000.
- [10] L. M. Ni, Y. H. Liu, Y. C. Lau, and A. P. Patil, "LANDMARC: indoor location sensing using active RFID," in *Proceedings of the 1st IEEE International Conference on Pervasive Computing and Communications (PerCom'03)*, pp. 407–415, Fort Worth, Tex, USA, March 2003.
- [11] T. S. Rappaport, *Wireless Communications: Principles and Practice*, Prentice Hall, 1st edition, 1996.
- [12] Laird Tech, <https://www.lairdtech.com/>.
- [13] Impinj, <http://www.impinj.com/>.
- [14] D. M. Dobkin, *The RF in RFID: Passive UHF RFID in Practice*, Newnes, Burlington, Mass, USA, 2008.
- [15] P. V. Nikitin, R. Martinez, S. Ramamurthy, H. Leland, G. Spiess, and K. V. S. Rao, "Phase based spatial identification of UHF RFID tags," in *Proceedings of the 4th Annual IEEE International Conference on RFID (RFID '10)*, pp. 102–109, Orlando, Fla, USA, April 2010.
- [16] S. Särkkä, V. V. Viikari, M. Huusko, and K. Jaakkola, "Phase-based UHF RFID tracking with nonlinear Kalman filtering and smoothing," *IEEE Sensors Journal*, vol. 12, no. 5, pp. 904–910, 2012.
- [17] Xilinx, <https://www.xilinx.com/>.
- [18] A. Povalac and J. Sebesta, "Phase difference of arrival distance estimation for RFID tags in frequency domain," in *Proceedings of the IEEE International Conference on RFID-Technologies and Applications*, pp. 188–193, September 2011.
- [19] C. Zhou and J. D. Griffin, "Accurate phase-based ranging measurements for backscatter RFID tags," *IEEE Antennas and Wireless Propagation Letters*, vol. 11, pp. 152–155, 2012.
- [20] R. E. Kalman, "A new approach to linear filtering and prediction problems," *Journal of Basic Engineering*, vol. 82, pp. 35–45, 1960.
- [21] X. Li, Y. Zhang, and M. G. Amin, "Multifrequency-based range estimation of RFID tags," in *Proceedings of the IEEE International Conference on RFID-Technologies and Applications*, pp. 147–154, April 2009.
- [22] EPCglobal, *Low Level Reader Protocol (LLRP)*, EPCglobal, 2010.
- [23] L. Yang, Y. Chen, X. Li, C. Xiao, M. Li, and Y. Liu, "Tagoram: real-time tracking of mobile RFID tags to high precision using COTS devices," in *Proceedings of the the 20th Annual International Conference on Mobile Computing and Networking (MobiCom '14)*, pp. 237–248, ACM, Maui, Hawaii, USA, September 2014.
- [24] M. Scherharufl, M. Pichler, D. Muller, A. Ziroff, and A. Stelzer, "Phase-of-arrival-based localization of passive UHF RFID tags," in *Proceedings of the IEEE MTT-S International Microwave Symposium Digest (IMS '13)*, pp. 1–3, IEEE, Seattle, Wash, USA, June 2013.